Silicon nitride waveguide polarization rotator and polarization beam splitter for chip-scale atomic systems

Kevin Gallacher, Paul F. Griffin, Erling Riis, et al.

View Online   **Export Citation**   **CrossMark**

ARTICLES YOU MAY BE INTERESTED IN

A simple imaging solution for chip-scale laser cooling
Applied Physics Letters **119**, 184002 (2021); https://doi.org/10.1063/5.0068725

Stand-alone vacuum cell for compact ultracold quantum technologies
Applied Physics Letters **119**, 124002 (2021); https://doi.org/10.1063/5.0061010

Deep learning-based design#of broadband GHz complex and random metasurfaces
APL Photonics **6**, 106101 (2021); https://doi.org/10.1063/5.0061571

AVS Quantum Science
SPECIAL TOPIC:
Quantum Networks: Past, Present and Future
SUBMIT TODAY!
Co-Published by AIP Publishing / AVS

Silicon nitride waveguide polarization rotator and polarization beam splitter for chip-scale atomic systems

View Online   Export Citation   CrossMark

Kevin Gallacher,[1,a] (iD) **Paul F. Griffin,**[2] (iD) **Erling Riis,**[2] **Marc Sorel,**[1,3] **and Douglas J. Paul**[1] (iD)

AFFILIATIONS

[1] James Watt School of Engineering, University of Glasgow, Glasgow G12 8LT, United Kingdom
[2] Department of Physics, SUPA, University of Strathclyde, Glasgow G4 0NG, United Kingdom
[3] TeCIP Institute, Scuola Superiore Sant'Anna, 56124 Pisa, Italy

[a] Author to whom correspondence should be addressed: kevin.gallacher@glasgow.ac.uk

ABSTRACT

The design, fabrication, and characterization of a silicon nitride waveguide polarization rotator and polarization beam splitter that operate with a polarization extinction ratio (PER) of ~30 dB at the rubidium atomic transition of 780 nm wavelength are demonstrated. These polarization devices are fabricated on the same chip using a self-aligned process for integration of the rib and ridge waveguide structures. The polarization rotator is based on the mode evolution approach using adiabatic tapers and demonstrates a PER of ≥20 dB over a 100 nm bandwidth (730–830 nm wavelengths) with an insertion loss (IL) ≤1 dB. The polarization beam splitter is based on a cascaded tapered asymmetric directional coupler with phase matching between the fundamental and higher order TM modes, whereas the TE mode is separated by the through port. This provides a PER ≥ 20 dB with IL ≤ 1 dB over a 50 nm bandwidth for the cross port and a PER ≥ 15 dB with an IL ≤ 1 dB over an 18 nm bandwidth for the through port. These polarization control waveguide devices will enable photonic integrated circuits for saturated absorption spectroscopy of atomic vapors for laser stabilization on-chip.

I. INTRODUCTION

Quantum technologies are benefiting from the size, weight, power, and cost reduction provided by silicon technology. A recent example is the commercially available chip-scale atomic clock, which utilized silicon MEMS to produce millimeter-sized vapor cells.[1,2] Research has now intensified on even smaller form factors and higher performance systems by leveraging photonic integrated circuits (PICs). For quantum systems based on thermal or cold atoms, such as Rb, silicon nitride (Si_3N_4) waveguides provide low loss propagation[3] and high-Q ring resonators.[4]

Si_3N_4 waveguides have recently demonstrated saturated absorption spectroscopy of Rb atoms using extreme mode-converting apodized gratings[5] and atomic-cladding waveguides.[6] In each of these approaches, however, the laser and circuitry for stabilization were off-chip. Saturated absorption spectroscopy is a technique where a counter-propagating pump and probe beam from the same laser are used to deplete the zero-velocity ground state of

atoms and reveal absorption dips that approach the natural linewidth of the atomic transition. This provides a Doppler-free feature for laser stabilization with thermal atoms.

Figure 1 shows a schematic diagram of an envisaged Si_3N_4 PIC for saturated absorption spectroscopy. This includes distributed feedback (DFB) lasers coupled to Si_3N_4 waveguides using a spot-size converter (SSC),[7] Si_3N_4 polarization rotator (PR) and polarization beam-splitter (PBS), Rb vapor MEMS cell, and Si photodetectors (PD). Utilizing a PR and PBS arrangement can create the required counter-propagating pump and probe with the advantage that the pump can be filtered from returning to the laser.[8] The pump and probe ratio could also be controlled by using a thermo-optically tuned splitter[9] at the input rather than a passive beam-splitter. Polarization control components are also essential for quantum communications sub-systems including quantum key distribution transmitter and receiver chips as well as repeaters.[10,11]
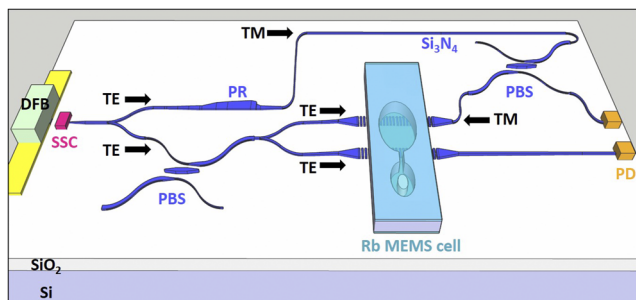
FIG. 1. A schematic diagram of a photonic integrated circuit for saturated absorption spectroscopy of rubidium atoms on-chip using Si_3N_4 waveguides. The key components include a Si_3N_4 waveguide polarization rotator (PR) and a polarization beam splitter (PBS), a distributed feedback laser (DFB), a Rb vapor MEMS cell, and photodetectors (PD).

PR and PBS waveguide devices have been extensively studied for creating polarization-insensitive PICs on the silicon-on-insulator (SOI) platform at telecommunication wavelengths.[12] With the current drive to combine SOI with the passive and nonlinear performance of Si_3N_4,[13] there have been recent PR[14,15] and PBS demonstrations.[16–23] Among these works, the smallest wavelength demonstration has been a PBS operating within the O-band (1260–1360 nm).[20] It is challenging to achieve small-footprint, high-performance Si_3N_4 polarization devices due to the lower refractive index and birefringence compared to SOI. It is, therefore, surprising that there have not been to date any demonstrations below the absorption band-edge of Si, where Si_3N_4 has a clear advantage. Shorter wavelength operation would also provide better compatibility with a number of single photon emitter sources,[24] underwater transmission applications,[25] and some free space transmission systems, such as those using satellites for quantum communications.[26]

In this work, we present a Si_3N_4 PR and PBS operating at the ^{87}Rb atomic transition of 780.24 nm. These devices are fabricated together on the same chip using a simple self-aligned process to integrate the required rib and ridge waveguide structures. The polarization rotator based on the mode evolution approach using adiabatic tapers demonstrates a polarization extinction ratio (PER) of ≥20 dB over 100 nm bandwidth with an insertion loss (IL) ≤ 1 dB. The polarization beam splitter is based on a cascaded tapered asymmetric directional coupler and provides a PER ≥ 20 dB and insertion loss ≤ 1 dB over 50 nm bandwidth for the cross port and a PER ≥ 15 dB with an IL ≤ 1 dB over an 18 nm bandwidth for the through port.

II. SELF-ALIGNED ETCH PROCESS FOR Si_3N_4 POLARIZATION ROTATOR AND POLARIZATION BEAM SPLITTER

The self-aligned fabrication process used to integrate both the PR and PBS on the same chip is detailed before discussing the design, modeling, and characterization. A Si_3N_4 layer of 200 nm thickness was deposited by low-pressure chemical vapor deposition (CVD) at 750 °C onto a 4 μm thick SiO_2 layer. The SiO_2 was thermally grown by wet oxidation at 1000 °C using a 150 mm

diameter Si wafer. Integrating rib and ridge waveguide structures required for the PR and PBS involved patterning with hydrogen silsesquioxane (HSQ) electron-beam lithography resist. After exposure to high-energy electrons, HSQ transitions to a network-like silica, which can then only be subsequently removed using hydrofluoric acid (HF).[27] This resistance to standard polymer cleaning then enables a self-aligned process for multiple etches when used in conjunction with other photo- or electron-beam resists (see Fig. S1 of the supplementary material). The rib waveguides were etched first to a target depth of 150 nm using a mixed gas (SF_6 and C_4F_8) process.[28] Next, to form the ridge waveguides, a polymethyl-methacrylate (PMMA) resist layer was patterned to open windows to etch the remaining Si_3N_4. The PMMA was then subsequently stripped using acetone followed by HSQ removal using dilute HF (10:1). As there is a significant difference in the etch rate between thermal SiO_2 and HSQ with HF, this results in only a few nanometers of undercutting.[29] Finally, a SiO_2 cladding layer of 1 μm thickness is added by plasma-enhanced CVD at 300 °C before the waveguides can be diced using a diamond saw and then optical facets polished.

III. Si_3N_4 POLARIZATION ROTATOR

There are three main strategies normally employed to realize waveguide polarization rotation devices: rotator waveguides,[30] cross-polarization coupling,[31] and mode evolution.[32] The simplest to implement is the mode evolution approach, where an adiabatic taper can efficiently convert between TM and TE modes.[33] This approach has the advantage that it is extremely fabrication tolerant and does not require any additional etching or lithography steps. To achieve this, an asymmetry has to be induced either vertically with a change of index and/or horizontally by structure. This can create supported modes where the dominant and non-dominant field components are equal. These hybridized modes then allow coupling when they have similar effective modal indices.[34] In this way, the waveguide width can be slowly tapered across the hybridization point to rotate the polarization. However, this usually results in a polarization conversion from a fundamental to higher order mode, requiring a subsequent higher order mode converter. To maintain symmetric waveguide cladding layers for compatibility, a cross-sectional asymmetry can be solely introduced by forming a rib waveguide structure.

A. TM0 to TE1 mode conversion

Figure 2 shows the calculated effective modal indices vs width for a 200 nm thick Si_3N_4 rib waveguide that has been etched 150 nm with top and bottom SiO_2 cladding. It is clear that the supported TE0 and TM0 modes are birefringent ($\Delta n \sim 0.1$) and there is an anti-crossing between the TM0 and TE1 modes at a waveguide width of ~975 nm, which is indicative of mode hybridization. The mode hybridization can be confirmed by analyzing the polarization ratio.[35] An eigenmode expansion solver (EME) was used to model a linear taper with input and output widths of 925 and 1025 nm, respectively. The calculated TM0 to TE1 polarization conversion efficiency (PCE) for three different wavelengths vs taper length is shown in Fig. 3(a). It is clear that, for taper lengths ≥750 μm, there is a PCE of ≥99% over an 100 nm bandwidth centered at 780 nm wavelength.
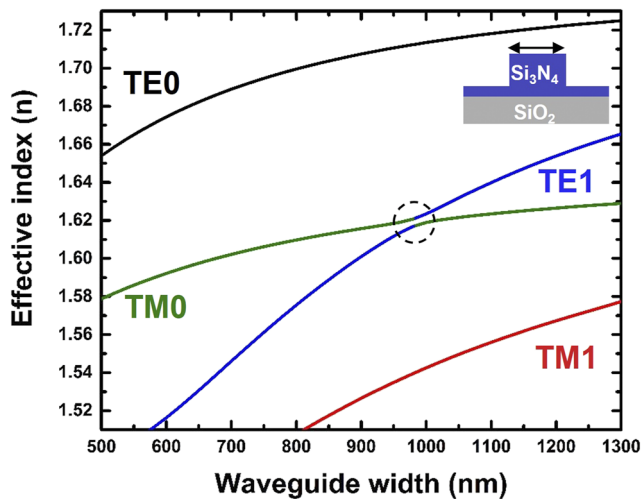
FIG. 2. The calculated effective modal indices vs the waveguide width for the supported modes in a 200 nm thick Si_3N_4 rib waveguide with a 150 nm etch at 780 nm wavelength. The mode hybridization point is indicated with a dashed circle.

B. TE1 to TE0 mode conversion

To provide TE1 to TE0 mode conversion, the higher order mode converters proposed by Chen *et al.* were utilized.[36,37] This approach is based on using an asymmetric taper structure that provides a different effective path length for the anti-phase components of the TE1 mode so that both components become in-phase and a TE0 mode is generated at the output. This approach has recently demonstrated a PR with record bandwidth and fabrication tolerance.[35] This was modeled by first optimizing a design that contained only two asymmetric tapers. The input (W_{TE1}) and output (W_{TE0}) width was fixed at 1.2 μm to ensure that the TE1 mode would be sufficiently far from any mode hybridization region. W_{TE0} was subsequently tapered to a width of 500 nm over a short distance (20 μm) so that any fraction of the TE1 mode not converted would be cut-off by a waveguide width that only supports a single mode. An EME solver (Lumerical) combined with a particle swarm optimization algorithm[38] with the figure of merit being the power transmitted to the fundamental TE0 mode at W_{TE0} was utilized.[35] There were four parameters initially optimized: W (2.42 μm), L_1 (11.58 μm), L_2 (13.07 μm), and L_3 (2.02 μm), which subsequently provided parameter bounds for a six asymmetric taper structure with parameters W_{12} (2.12 μm), W_{22} (2.82 μm), W_{23} (1.58 μm), L_{12} (6.47 μm), L_{22} (10.64 μm), and L_{23} (0.2 μm). Figure 3(b) shows the modeled TE1 to TE0 conversion efficiency for the optimized two and six asymmetric taper structures. The six asymmetric taper structure demonstrates a peak conversion efficiency of ~95% at 780 nm wavelength. There is ≥80% conversion efficiency over 150 nm bandwidth (725–875 nm). The complete waveguide PR design consists of a linear adiabatic taper (TM0 to TE1) followed by an asymmetric taper structure (TE1 to TE0).

C. PR fabrication and characterization

Si_3N_4 PRs consisting of an adiabatic 750 μm long linear taper for highly efficient TM0 to TE1 mode conversion followed by the
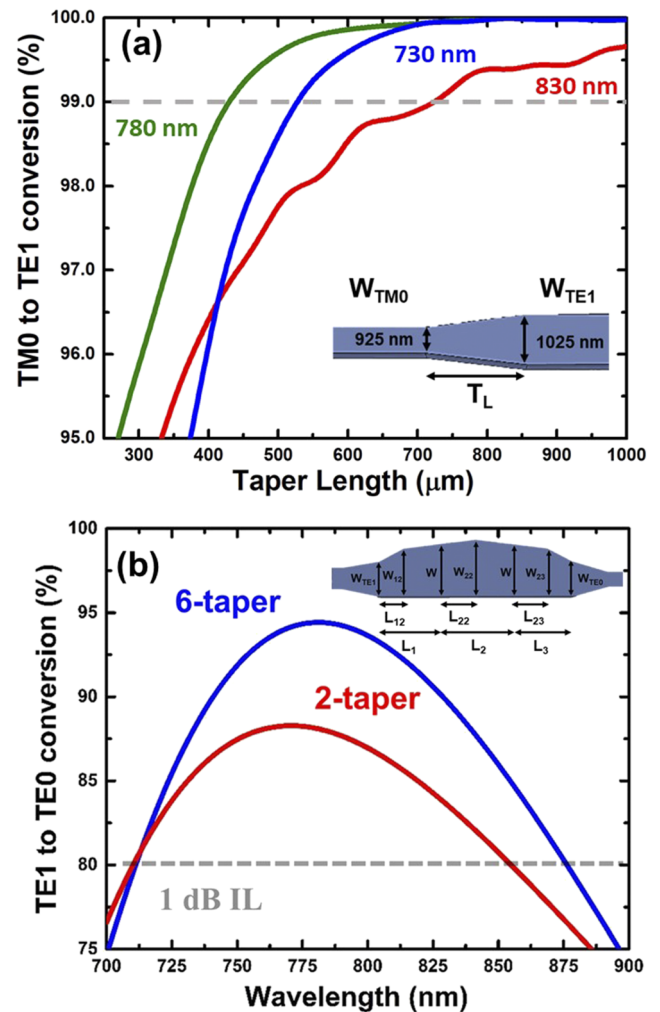

FIG. 3. (a) The modeled TM0 to TE1 mode conversion efficiency vs taper length (T_L) for a Si_3N_4 rib waveguide that is linearly tapered from an input width (W_{TM0}) of 925 nm to an output width (W_{TE1}) of 1025 nm. The calculated wavelengths consist of 730, 780, and 830 nm wavelengths. (b) The simulated TE1 to TE0 conversion efficiency for the optimized higher order mode converter consisting of two or six asymmetric tapers (see text for W and L dimensions) modeled with an eigenmode expansion solver (Lumerical). The 1 dB insertion loss point is highlighted by a dashed line.

optimized six asymmetric taper TE1 to TE0 higher order mode converter were fabricated using the self-aligned process previously discussed. A surface profiler was used to measure the actual etch depth achieved for the rib waveguide structure (~160 nm). To enable straightforward characterization of the IL, the PR was fabricated onto one arm of a y-splitter (50:50 beam splitter) with the other arm acting as the reference waveguide. Characterization was then performed using a setup consisting of a titanium sapphire laser (SolsTiS M Squared Lasers), which is tunable from 730 to 870 nm wavelengths with a 50 kHz linewidth. The laser was initially incident upon a mechanical chopper that was used in conjunction with a lock-in amplifier to reduce noise from ambient light. The polarization was

then precisely set using a polarimeter in combination with a half-wave plate and a high extinction linear polarizer (60 dB) to ensure only a TM fundamental mode was excited at the input. End-fire coupling to the waveguides was then achieved using a high magnification objective lens (40×), producing a ~1 μm diameter spot size. At the output, another objective lens was used to collect before the polarization axis of another identical polarizer was adjusted for the detection of the transmitted TE0 and TM0 modes by a photodetector (see Fig. S2 of the supplementary material). The PER and IL are defined as

$$PER = -10 \times \log_{10}\left(\frac{TM_{in} \rightarrow TM_{out}}{TM_{in} \rightarrow TE_{out}}\right) \tag{1}$$

and

$$IL = -10 \times \log_{10}(TM_{ref} \rightarrow TE_{out}). \tag{2}$$

Figure 4 shows the measured PER and IL as a function of the wavelength. Over the wavelength range where the IL ≤ 1 dB (730–840 nm), the PER is ≥17.5 dB. The PER at 780 nm wavelength is ~27.5 dB. Above 840 nm, the IL increases, which is most likely a consequence of the 10 nm over-etch compared to the nominal design. This device, however, still demonstrates an operational bandwidth of over 100 nm, which is more than sufficient to be used in a PIC for atomic vapor applications. The two previous Si3N4 demonstrations[14,15] that operate at 1550 nm are based on an augmented low-index-guiding (ALIG) structure consisting of a Si3N4/Si dual-core waveguide. This approach benefits from higher birefringence but cannot operate below the absorption band-edge of Si.
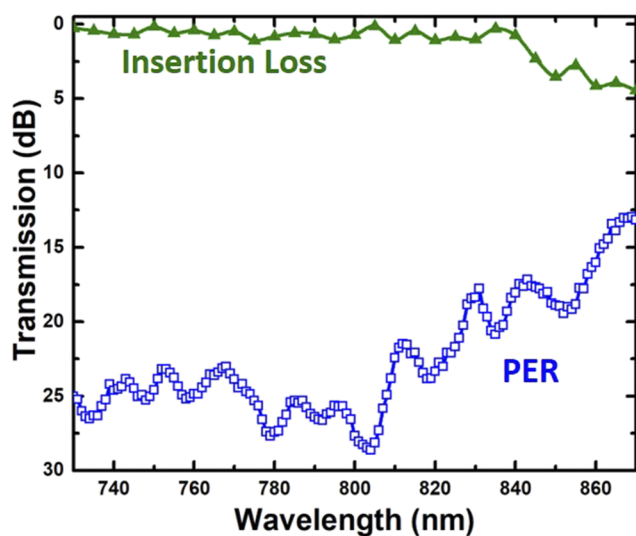

FIG. 4. The experimentally measured polarization extinction ratio (PER) and insertion loss (IL) for the fabricated Si3N4 waveguide polarization rotator consisting of a 750 μm long linear taper (TM0–TE1) followed by the ~26 μm long optimized six asymmetric taper (TE1–TE0) as a function of the wavelength.

IV. Si3N4 POLARIZATION BEAM SPLITTER

PBS have been demonstrated on the Si3N4 platform using Mach–Zehnder interferometers (MZIs),[17,18] multi-modal interferometers (MMIs),[19,22,23] and directional couplers (DCs).[16,20] DCs have been the most popular choice on the SOI platform[39] with even basic designs involving coupling between symmetric waveguides providing high PER due to the large geometric birefringence that can be induced.[40] A DC is composed of two parallel waveguides where light can be coupled evanescently from one waveguide to another by having an appropriate gap spacing and coupling length. This can provide polarization splitting when there is a significant difference in the cross-over lengths for the supported TM and TE modes. To achieve higher performance and smaller footprints, designs have focused on generating cross-coupling of only one polarization by utilizing an asymmetric directional coupler (ADC).[41,42] This works by having two parallel waveguides of different widths, where one of the supported polarization modes is prevented from efficiently phase matching. This approach is interesting for the Si3N4 platform since it does not provide a high level of birefringence. Another benefit of an ADC is that it can allow higher order mode coupling, which provides multiple design parameters for engineering strong phase matching of only one polarization.[43]

A. TM0 to TM1 mode phase matching

Figure 5(a) shows the calculated effective modal indices vs width for a 200 nm thick Si3N4 ridge waveguide that has both top and bottom SiO2 cladding. It is clear that, for waveguide widths of 502 and 1300 nm, phase matching ($n_{eff0} = n_{eff1}$) can be satisfied between the TM0 and TM1 modes at a wavelength of 780 nm. On the other hand, it can be seen that phase matching does not occur between the TE0 and TE1 modes. An ADC-PBS based on this approach will selectively cross couple only the TM polarized guided mode, whereas the TE mode will pass straight through unperturbed. This guarantees a high PER for the cross-coupling port but the IL and PER of the through port, which are intrinsically linked, will be severely compromised for lithography errors greater than 5 nm (see Fig. S3 of the supplementary material). One way to make the design more fabrication tolerant is to utilize slowly width-varying tapered DCs that are less sensitive to coupling length (L_c) variations.[44] Figure 5(b) shows the calculated effective indices vs width for the supported TM0 and TM1 modes at 730, 780, and 830 nm wavelengths. The optimum widths for phase matching between the TM0 and TM1 modes at 780 nm do not translate to the other calculated wavelengths. This effect is more strongly exasperated at shorter wavelengths due to the bulk dispersion of Si3N4. Therefore, slowly tapering over a range of waveguide widths will increase the bandwidth and ensure high performance at the center wavelength.

B. Tapered asymmetric directional coupler

Figure 6(a) shows a top-down schematic diagram of the proposed cascaded tapered ADC-PBS. By tapering the through and cross waveguide widths in an opposite direction from the multimodal bridge waveguide allows the gap spacing for coupling to remain fixed. Compared to the previous demonstration of this approach on SOI using only two single-mode waveguides,[44] here,
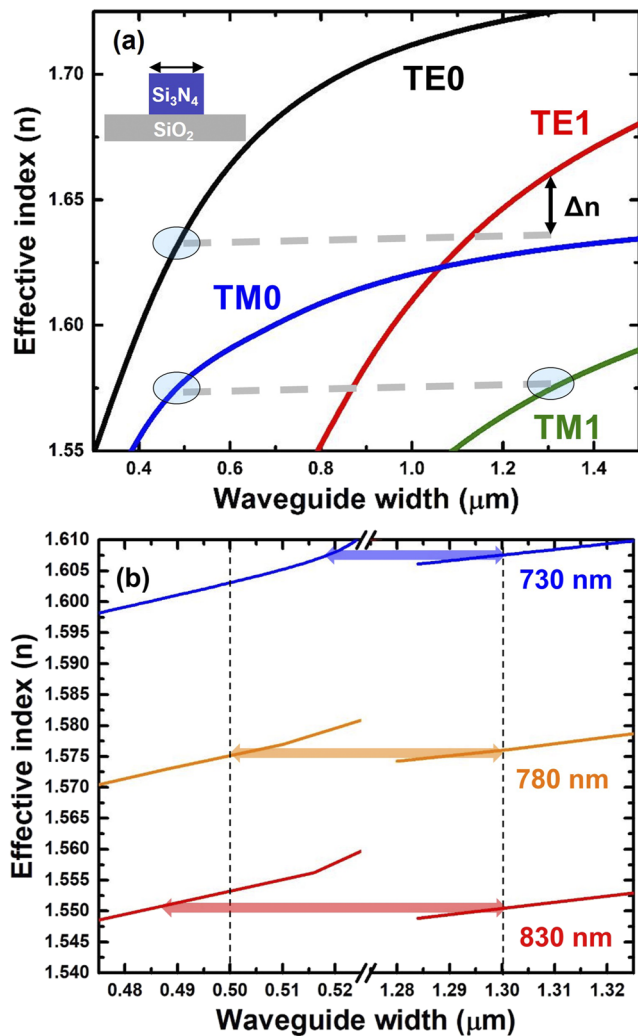
FIG. 5. (a) The calculated effective modal indices vs the waveguide width for the supported modes in a 200 nm thick Si$_3$N$_4$ ridge waveguide at 780 nm wavelength. The horizontal dashed lines indicate the widths required for phase matching between the TM0 and TM1 modes. (b) The calculated effective modal indices vs the waveguide width for the supported TM0 and TM1 modes at 730, 780, and 830 nm wavelengths. The TM0 modes are shown on the left of the axis break, whereas the TM1 modes are shown on the right. The vertical dashed lines indicate the waveguide widths required for phase matching at 780 nm.
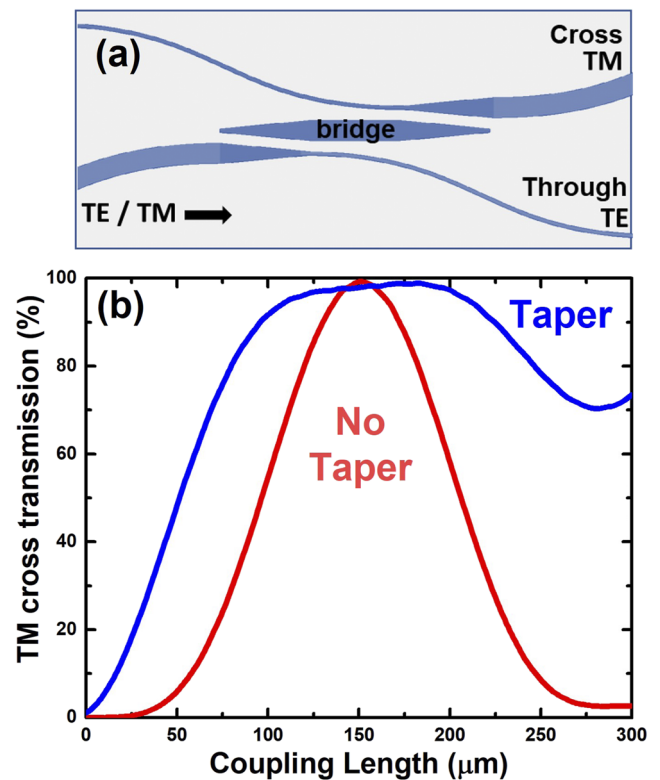

FIG. 6. (a) A top-down schematic diagram (not to scale) of the proposed cascaded tapered asymmetric directional coupler polarization beam splitter (ADC-PBS). (b) The simulated TM0 cross transmission for an ADC-PBS with and without tapering vs coupling length at 780 nm wavelength.

a third multi-modal bridge waveguide is required in order to selectively couple only one polarization using higher order mode conversion due to the lower birefringence. The consequence of this bridge waveguide is that it then necessitates two distinct cross-coupling tapered regions due to the lack of symmetry. The design of the device consists of the through and cross waveguide widths tapered from 475 to 525 nm, along with the bridge tapered from 1275 to 1325 nm in the opposite direction. The bridge also contains a 15 μm long straight waveguide section that is used in conjunction with 100 μm radius S-bends to offset the two distinct cross-coupling

regions. An EME solver was used to model the TM0 cross transmission vs L_c for the cascaded tapered ADC-PBS and a non-tapered design consisting of fixed widths for the through and cross waveguides (502 nm) along with the multi-modal bridge (1300 nm) each separated by a gap spacing of 500 nm [see Fig. 6(b)]. It is clear that the addition of the tapers decreases the sensitivity of the TM0 cross transmission to changes in the L_c, which will increase fabrication tolerance.

C. PBS fabrication and characterization

A Si$_3$N$_4$ cascaded tapered ADC-PBS with two 150 μm long coupling sections was fabricated using the self-aligned process as previously discussed. Figure 7(a) shows a scanning electron microscope image of the fabricated device. False color is used to highlight the rib and ridge Si$_3$N$_4$ waveguide sections and windows that have been patterned and etched to realize the ridge waveguide structure. Characterization was performed using the setup discussed earlier by exciting either the fundamental TE or TM mode at the input of the through port and then measuring the transmission of each polarization at the through and cross output ports. To measure the output of each port separately, they was an offset of 50 μm and a pin hole aperture was used after collection by the objective lens. Figure 7(b) shows the experimentally measured transmission vs wavelength of
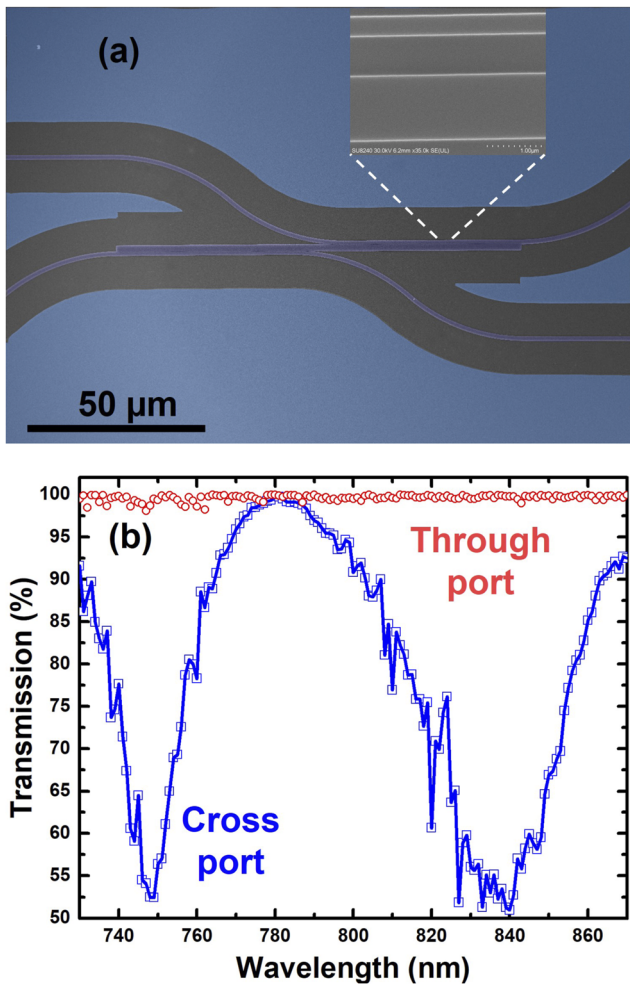
FIG. 7. (a) A scanning electron microscope (SEM) image of a fabricated Si$_3$N$_4$ waveguide cascaded tapered asymmetric directional coupler. The inset shows a higher magnification image of the coupling section between the single and multi-modal bridge waveguides. (b) The experimentally measured transmission of the through port when injecting a TE mode and the cross port when injecting a TM mode as a function of the wavelength.

the through port when injecting a TE mode and the cross port for an injected TM mode. As expected when injecting a TE mode, negligible cross-coupling occurs even across the full wavelength range of the setup since there is no phase matching to the bridge waveguide. In contrast, the TM mode, which is designed to cross couple, is far more sensitive to a change in wavelength. It is clear that there is ~100% transmission achieved at 780 nm wavelength and ≥80% over a 50 nm bandwidth (760–810 nm wavelengths). To calculate the PER and IL for the PBS, the measured spectral responses of the output from the through and cross ports are normalized compared to a reference waveguide for both polarization states. The PER and IL are then defined as

$$PER_{TE,TM} = -10 \times \log_{10}\left(\frac{T_{Through,Cross}}{T_{Cross,Through}}\right) \qquad (3)$$

and

$$IL_{TE,TM} = -10 \times \log_{10}\left(T_{Through,Cross}\right), \qquad (4)$$

where $T_{Through}$ and T_{Cross} are the transmission of the through and cross output ports when injecting either a TE or TM mode at the input of the through port. As shown in Fig. 8(a), the PER for the cross port is almost >20 dB across the full 140 nm measurement range with it peaking at 30 dB close to 780 nm wavelength. This broadband PER is expected since there is negligible cross-coupling of the TE mode. The main parameter of interest for the cross port is the IL, which is ≤1 dB between 760 and 810 nm wavelengths. Figure 7(b) shows the PER for the through port with a peak of
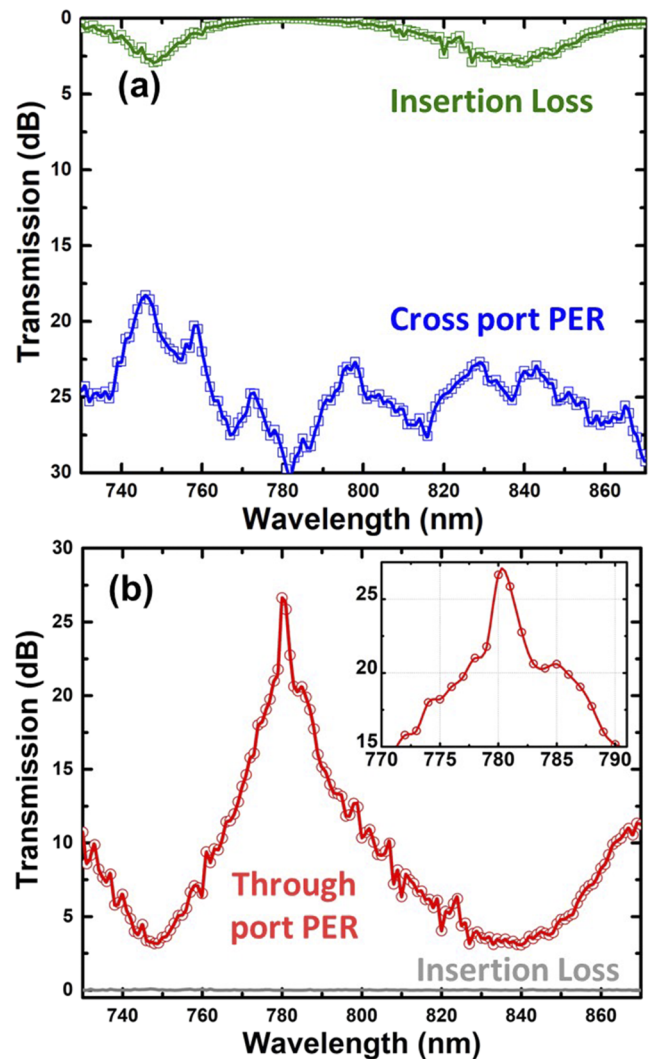

FIG. 8. (a) The experimentally measured polarization extinction ratio (PER) and insertion loss (IL) for the cross port of the fabricated Si$_3$N$_4$ waveguide polarization beam splitter (PBS) as a function of the wavelength. (b) The experimentally measured PER of the through port vs wavelength for the fabricated PBS. The inset shows, in more detail, the wavelength range where the PER ≥ 15 dB.

TABLE I. Comparison of experimentally demonstrated Si_3N_4 waveguide polarizing beam splitters.

Structure	PER (dB)	IL (dB)	BW (nm)	Wavelength (nm)	Length (μm)	References
MZI w/active control	>20	<0.1	38	1536–1576	1000	17
MZI	>20	<1.5	80	1530–1610	113	18
MMI (ALIG)	>17 (through)/>25 (cross)	<1.0	35	1530–1565	4.8	19
MMI	>20	<1.0	100	1525–1625	80	22
MMI	>30	~1.1	22	1550–1572	820	23
3D-DC	>16	<1.0	30	1535–1565	800	16
Phase controlled DC	>10	<0.6	95	1260–1355	136	20
Cascaded tapered ADC	>15 (through)/>20 (cross)	<1.0	18 (through)/50 (cross)	760–810	315	This work

27.5 dB at 780 nm wavelength. The PER is ≥15 dB for a bandwidth of 18 nm [see the inset of Fig. 7(b)]. One way to improve the bandwidth of the through port would be to filter the remaining fraction of the TM mode that is not cross-coupled by cascading the device. This would constitute minimal added IL since the TE mode is unperturbed but would increase the overall footprint.

D. Discussion

Finally, the performance of the PBS is compared to the previous experimental Si_3N_4 demonstrations given in Table I. These demonstrations have been at telecommunication wavelengths with the smallest wavelength being a phase-controlled DC-PBS operating within the O-band (1260–1360 nm).[20] It is clear that the length of these devices is much larger compared to what can be achieved with the state of art SOI PBS due to the lower birefringence. It is only the ALIG device composed of a Si_3N_4/Si dual-core that has a length <10 μm.[19] This work represents the first demonstration below the Si absorption band edge, where Si_3N_4 provides a clear advantage. The PER, IL, and length are comparable to what has been achieved with the telecommunication-based devices. The operational bandwidth of 50 nm for the cross port and 18 nm for the through port compare favourably when analyzed as a fractional bandwidth ($B_F = \Delta_f/f_c$).

V. CONCLUSION

A Si_3N_4 waveguide polarization rotator and polarization beam splitter that operates at the [87]Rb atomic transition of 780.24 nm is presented. These devices are fabricated together on the same chip using a simple self-aligned process for integration of the required rib and ridge waveguide structures. The polarization rotator based on the mode evolution approach using adiabatic tapers demonstrates a polarization extinction ratio (PER) of ≥20 dB over 100 nm bandwidth (730–830 nm wavelengths) with an insertion loss (IL) ≤ 1 dB. The polarization beam splitter is based on a cascaded tapered asymmetric directional coupler design with phase matching engineered between the fundamental and higher order TM modes, whereas the TE mode is separated by the through port. This approach provides a PER ≥ 20 dB over 50 nm bandwidth for the cross port and a PER ≥ 15 over 18 nm for the through port. These polarization control waveguide devices can enable photonic integrated circuits for saturated absorption spectroscopy of atomic vapors for laser stabilization on-chip.

SUPPLEMENTARY MATERIAL

See the supplementary material for further details regarding the self-aligned etch process, experimental setup, and fabrication tolerance of the asymmetric directional coupler polarization beam splitter without tapering.

AUTHOR DECLARATIONS

Conflict of Interest

The authors have no conflicts to disclose.

DATA AVAILABILITY

The data that support the findings of this study are available from the corresponding author upon reasonable request.

REFERENCES

[1]J. Kitching, "Chip-scale atomic devices," Appl. Phys. Rev. **5**, 031302 (2018).

[2]L. Liu, D.-S. Lü, W.-B. Chen, T. Li, Q.-Z. Qu, B. Wang, L. Li, W. Ren, Z.-R. Dong, J.-B. Zhao, W.-B. Xia, X. Zhao, J.-W. Ji, M.-F. Ye, Y.-G. Sun, Y.-Y. Yao, D. Song, Z.-G. Liang, S.-J. Hu, D.-H. Yu, X. Hou, W. Shi, H.-G. Zang, J.-F. Xiang, X.-K. Peng, and Y.-Z. Wang, "In-orbit operation of an atomic clock based on laser-cooled Rb-87 atoms," Nat. Commun. **9**, 2760 (2018).

[3]A. Z. Subramanian, P. Neutens, A. Dhakal, R. Jansen, T. Claes, X. Rottenberg, F. Peyskens, S. Selvaraja, P. Helin, B. Du Bois, K. Leyssens, S. Severi, P. Deshpande, R. Baets, and P. Van Dorpe, "Low-loss singlemode PECVD silicon nitride photonic wire waveguides for 532–900 nm wavelength window fabricated within a CMOS pilot line," IEEE Photonics J. **5**, 2202809 (2013).

[4]M. Sinclair, K. Gallacher, M. Sorel, J. C. Bayley, E. McBrearty, R. W. Millar, S. Hild, and D. J. Paul, "1.4 million Q factor Si_3N_4 micro-ring resonator at 780 nm wavelength for chip-scale atomic systems," Opt. Express **28**, 4010–4020 (2020).

[5]M. T. Hummon, S. Kang, D. G. Bopp, Q. Li, D. A. Westly, S. Kim, C. Fredrick, S. A. Diddams, K. Srinivasan, V. Aksyuk, and J. E. Kitching, "Photonic chip for laser stabilization to an atomic vapor with 10^{-11} instability," Optica **5**, 443–449 (2018).

[6] R. Zektzer, N. Mazurski, Y. Barash, and U. Levy, "Nanoscale atomic suspended waveguides for improved vapour coherence times and optical frequency referencing," Nat. Photonics 15, 772 (2021).

[7] K. Gallacher, M. Sinclair, R. W. Millar, O. Sharp, F. Mirando, G. Ternent, G. Mills, B. Casey, and D. J. Paul, "Integrated DFB lasers on Si$_3$N$_4$ photonic platform for chip-scale atomic systems," in 2019 Conference on Lasers and Electro-Optics (CLEO) (IEEE, 2019), pp. 1–2.

[8] K. B. Macadam, A. Steinbach, and C. Wieman, "A narrow-band tunable diode-laser system with grating feedback, and a saturated absorption spectrometer for Cs and Rb," Am. J. Phys. 60, 1098–1111 (1992).

[9] H. Nejadriahi, A. Friedman, R. Sharma, S. Pappert, Y. Fainman, and P. Yu, "Thermo-optic properties of silicon-rich silicon nitride for on-chip applications," Opt. Express 28, 24951–24960 (2020).

[10] M. Minder, M. Pittaluga, G. L. Roberts, M. Lucamarini, J. F. Dynes, Z. L. Yuan, and A. J. Shields, "Experimental quantum key distribution beyond the repeaterless secret key capacity," Nat. Photonics 13, 334–338 (2019).

[11] H. Semenenko, P. Sibson, A. Hart, M. G. Thompson, J. G. Rarity, and C. Erven, "Chip-based measurement-device-independent quantum key distribution," Optica 7, 238–242 (2020).

[12] D. Dai, "Advanced passive silicon photonic devices with asymmetric waveguide structures," Proc. IEEE 106, 2117–2143 (2018).

[13] T. Sharma, J. Wang, B. K. Kaushik, Z. Cheng, R. Kumar, Z. Wei, and X. Li, "Review of recent progress on silicon nitride-based photonic integrated circuits," IEEE Access 8, 195436–195446 (2020).

[14] W. D. Sacher, Y. Huang, L. Ding, T. Barwicz, J. C. Mikkelsen, B. J. F. Taylor, G.-Q. Lo, and J. K. S. Poon, "Polarization rotator-splitters and controllers in a Si$_3$N$_4$-on-SOI integrated photonics platform," Opt. Express 22, 11167–11174 (2014).

[15] X. Sun, M. Z. Alam, J. S. Aitchison, and M. Mojahedi, "Polarization rotator based on augmented low-index-guiding waveguide on silicon nitride/silicon-on-insulator platform," Opt. Lett. 41, 3229–3232 (2016).

[16] J. Feng and R. Akimoto, "A three-dimensional silicon nitride polarizing beam splitter," IEEE Photonics Technol. Lett. 26, 706–709 (2014).

[17] J. Feng and R. Akimoto, "Silicon nitride polarizing beam splitter with potential application for intersubband-transition-based all-optical gate device," Jpn. J. Appl. Phys. 54, 04DG08 (2015).

[18] S. Gao, Y. Wang, K. Wang, and E. Skafidas, "Low-loss and broadband 2 × 2 polarization beam splitter based on silicon nitride platform," IEEE Photonics Technol. Lett. 28, 1936–1939 (2016).

[19] X. Sun, J. S. Aitchison, and M. Mojahedi, "Realization of an ultra-compact polarization beam splitter using asymmetric MMI based on silicon nitride/silicon-on-insulator platform," Opt. Express 25, 8296–8305 (2017).

[20] S. Guerber, C. Alonso-Ramos, D. Benedikovic, E. Duran-Valdeiglesias, X. Le Roux, N. Vulliet, E. Cassan, D. Marris-Morini, C. Baudot, F. Boeuf, and L. Vivien, "Broadband polarization beam splitter on a silicon nitride platform for O-band operation," IEEE Photonics Technol. Lett. 30, 1679–1682 (2018).

[21] B. Bhandari, C.-S. Im, O. R. Sapkota, and S.-S. Lee, "Highly efficient broadband silicon nitride polarization beam splitter incorporating serially cascaded asymmetric directional couplers," Opt. Lett. 45, 5974–5977 (2020).

[22] R. Kudalippalliyalil, T. E. Murphy, and K. E. Grutter, "Low-loss and ultra-broadband silicon nitride angled MMI polarization splitter/combiner," Opt. Express 28, 34111–34122 (2020).

[23] J. Zhan, J. Brock, S. Veilleux, and M. Dagenais, "Silicon nitride polarization beam splitter based on polarization-independent MMIs and apodized Bragg gratings," Opt. Express 29, 14476–14485 (2021).

[24] L. Sapienza, M. Davanço, A. Badolato, and K. Srinivasan, "Nanoscale optical positioning of single quantum dots for bright and pure single-photon emission," Nat. Commun. 6, 7833 (2015).

[25] F. Hufnagel, A. Sit, F. Grenapin, F. Bouchard, K. Heshami, D. England, Y. Zhang, B. J. Sussman, R. W. Boyd, G. Leuchs, and E. Karimi, "Characterization of an underwater channel for quantum communications in the Ottawa River," Opt. Express 27, 26346–26354 (2019).

[26] J. G. Rarity, P. R. Tapster, P. M. Gorman, and P. Knight, "Ground to satellite secure key exchange using quantum cryptography," New J. Phys. 4, 82 (2002).

[27] U. Griskeviciute, R. W. Millar, K. Gallacher, J. Valente, and D. J. Paul, "Ge-on-Si waveguides for sensing in the molecular fingerprint regime," Opt. Express 28, 5749–5757 (2020).

[28] K. Gallacher, R. W. Millar, U. Griškevičiūtė, L. Baldassarre, M. Sorel, M. Ortolani, and D. J. Paul, "Low loss Ge-on-Si waveguides operating in the 8–14 μm atmospheric transmission window," Opt. Express 26, 25667–25675 (2018).

[29] V. Passi, A. Lecestre, C. Krzeminski, G. Larrieu, E. Dubois, and J.-P. Raskin, "A single layer hydrogen silsesquioxane (HSQ) based lift-off process for germanium and platinum," Microelectron. Eng. 87, 1872–1878 (2010).

[30] C. Alonso-Ramos, S. Romero-García, A. Ortega-Moñux, I. Molina-Fernández, R. Zhang, H. G. Bach, and M. Schell, "Polarization rotator for InP rib waveguide," Opt. Lett. 37, 335–337 (2012).

[31] Y. Fei, L. Zhang, T. Cao, Y. Cao, and S. Chen, "Ultracompact polarization splitter-rotator based on an asymmetric directional coupler," Appl. Opt. 51, 8257–8261 (2012).

[32] M. R. Watts and H. A. Haus, "Integrated mode-evolution-based polarization rotators," Opt. Lett. 30, 138–140 (2005).

[33] D. X. Dai, J. Bauters, and J. E. Bowers, "Passive technologies for future large-scale photonic integrated circuits on silicon: Polarization handling, light non-reciprocity and loss reduction," Light: Sci. Appl. 1, e1 (2012).

[34] D. Dai and H. Wu, "Realization of a compact polarization splitter-rotator on silicon," Opt. Lett. 41, 2346–2349 (2016).

[35] K. Gallacher, R. W. Millar, U. Griškevičiūtė, M. Sinclair, M. Sorel, L. Baldassarre, M. Ortolani, R. Soref, and D. J. Paul, "Ultra-broadband mid-infrared Ge-on-Si waveguide polarization rotator," APL Photonics 5, 026102 (2020).

[36] D. Chen, X. Xiao, L. Wang, Y. Yu, W. Liu, and Q. Yang, "Low-loss and fabrication tolerant silicon mode-order converters based on novel compact tapers," Opt. Express 23, 11152–11159 (2015).

[37] D. Chen, X. Xiao, L. Wang, W. Liu, Q. Yang, and S. Yu, "Highly efficient silicon optical polarization rotators based on mode order conversions," Opt. Lett. 41, 1070–1073 (2016).

[38] Y. Zhang, S. Yang, A. E.-J. Lim, G.-Q. Lo, C. Galland, T. Baehr-Jones, and M. Hochberg, "A compact and low loss Y-junction for submicron silicon waveguide," Opt. Express 21, 1310–1316 (2013).

[39] D. Dai, "Silicon polarization beam splitter based on an asymmetrical evanescent coupling system with three optical waveguides," J. Lightwave Technol. 30, 3281–3287 (2012).

[40] I. Kiyat, A. Aydinli, and N. Dagli, "A compact silicon-on-insulator polarization splitter," IEEE Photonics Technol. Lett. 17, 100–102 (2005).

[41] H. Wu, Y. Tan, and D. Dai, "Ultra-broadband high-performance polarizing beam splitter on silicon," Opt. Express 25, 6069–6075 (2017).

[42] J. R. Ong, T. Y. L. Ang, E. Sahin, B. Pawlina, G. F. R. Chen, D. T. H. Tan, S. T. Lim, and C. E. Png, "Broadband silicon polarization beam splitter with a high extinction ratio using a triple-bent-waveguide directional coupler," Opt. Lett. 42, 4450–4453 (2017).

[43] D. Dai, L. Liu, S. Gao, D.-X. Xu, and S. He, "Polarization management for silicon photonic integrated circuits," Laser Photonics Rev. 7, 303–328 (2013).

[44] D. Chen, X. Xiao, L. Wang, G. Gao, W. Liu, and Q. Yang, "Broadband, fabrication-tolerant polarization beam splitters based on a tapered directional coupler," IEEE Photonics Technol. Lett. 28, 2074–2077 (2016).